Capabilities of existing USA civilian radars to detect plumes

Part II

D. Zrnic, V. Melnikov, and P. Zhang

This is the second part of a report prepared for the Oak Ridge National Laboratory. It contains 1) discussion of X-band (3 cm wavelength) radars' capabilities for detection of plumes; 2) example of smoke plume from a large wild fire detected by a WSR-88D (KHDS) in New Mexico, and 3) plumes from fireworks in Norman OK, detected by the NOAA/NSSL X-band polarimetric radar and the TDWR.

Capabilities of existing USA civilian radars to detect plumes

Part II

D. Zrnic, V. Melnikov, P. Zhang

1. Introduction

This second part of a report prepared for DOE further discusses the capabilities of the US civilian radars to detect smoke plumes and weak weather signals. We continue discussion of the 3-cm wavelength radars and present examples of storms observed simultaneously by the WSR-88D and 3 cm mobile radars.

Brief summary about the short wavelength cloud radars is included in a comparative table with the 3 cm wavelength radars.

We also present values of the polarimetric variables from smoke plumes and fireworks. From these we make inferences about the added value that the polarimetric variables bring to the detection of plumes. In one case we compare observation of the same plume with the TDWR and WSR-88D radars.

2. Short wavelength radars

Herein we replicate Table 2 from the report I (Zrnic at al. 2017) but add five more X band radars and three cloud radars.

Table 1. Characteristics of radars at different wavelengths.

Radar	λ cm	P_t kW	θ_1 deg	D_a m	g dB	τ μs	Noise dBm	$2L_a$ dB	Z_{10} dBZ	r_0 km
WSR-88D[1]	10.7	237[1]	1	8.4	46	1.57[2] 4.71	-114	0.8	-24 -34	10
TDWR	5.45	250	1	8.4	50	1.1		1	-25.6	10
XERES[1]	3.2	100[1]	1	2.5	46	1	-112	10	-19.5	10
RaXPol[3]	3.08	20	1	2.4	44.5	1			-13	10
UMasXPol[4]	3.18	12.5	1.25	1.8	45	1	-112	7	-13.5	10
PX-1000[5]	3.14	0.1	1.8	1.2	38.5	1	-112	7	2	10
CASA[6]	3.18	8	1.8	1.2	38	1	-112	7	- 1	10
DOW[7]	3.15	250	0.93	2.6	46.1	1	-112	10	-23.7	10
MMCR-8[8]	0.84	100	0.3	1.8		1			-31	10
CSR[9]	0.3	1.7	0.6x0.8		46.4	1			-11.7	10
CSR[10]	0.3	1.7	0.3		55	1			-28.9	10
CPR[11]	0.3		0.12	1.85		3.3			-33	10

[1)] Both the WSR-88D and XERES have dual polarization hence the powers and the detection capabilities are per channel. For XERES a loss of 10 dB is assumed but not verified.

[2)] The pulse widths are measured between the -6 dB points with respect to the pulse peak.

[3)] This is rapid scanning radar that uses frequency diversity (4 frequencies). The -13 dB is the value sited by (Snyder et al. 2010) and it implies a loss of 7 dB. A. Pazmany from ProSensing (Radar manufacturer) computed the detectability of -14 dBZ a values very close to the one in the Table.

[4)] This is U. Mass dual pol radar. Power is per channel (see Snyder et al. 2010).

[5] This radar has pulse compression (peak Pt=1.5 kW with up to 15 μs pulse or 100 W with up to 100 μs pulse). Compression used is 60 times, pulse width is 1 μs, 100W peak total power (per channel 50 W); a loss of 7 dB is assumed. See Fig 1 for an example and reconciliation of Z_{10}.
[6] This is CASA radar (Junyent et al. 2010). 8 kW peak power is per channel; a 7 dB loss is assumed.
[7] This radar belongs to the Center for Sever Weather Research (CSWR). The power is per channel; a 10 dB loss is assumed as it has similar characteristic as XERES.
[8] This is the 8 mm wavelength cloud radar (MMCR-8) operated by the DOE Atmospheric Radiation Measurement (ARM) program; A. Pazmany (ProSensing) provided the information.
[9] This is NASA's Cloud Radar System airborne version (all the values are from Li et al. 2004).
[10] This is NASA's Cloud Radar System ground version (all the values are from Li et al. 2004).
[11] This is NASA's Cloud Profiling Radar on a satellite.

The values in the Table 1 are either obtained from the literature, or ProSensing (A. Pazmany), or ROC (R. Ice), or are our best estimates. The -112 dBm noise level has been estimated for the XERES but the other listed values are assumed. Blanks indicate that the values were not found in the literature. In such cases we have made estimates of Z_{10} by properly scaling parameters such as gains and beamwidth, and assuming the same noise level and losses (see eq 2 in the Zrnic et al 2017), or we have used published values, or personal information. Thus the results could be off by a couple of dB which does not alter the relative merits of these comparisons. The same pulse width is used for inter comparisons of the X band radars except for the PX-1000 a pulse compression is considered.

The detection capabilities are valid if there is no precipitation along the propagation path. Rain presence degrades detection to the point that the signal can be totally lost as quantified in Zrnic et al. (2017).

a) *X-band radars*

All listed 3 cm wavelength radars are mobile on trucks and can be used on the fly. Typically it takes but few minutes to level the truck and start data collection. Without leveling the data collection can begin immediately after the truck has stopped.

Some of the X-band radars use pulse compression to effectively increase the transmitted power while preserving resolution. The example is the PX-1000 radar (Table 1) which was designed by the University of Oklahoma. It has a solid state transmitter hence uses pulse compression for distant ranges (>10 km) and a fill in pulse at short range. The detection capability assumes a compressed pulse of 1 μs and a compression ratio of 60 so that the measurement with pulse compression can be made at 10 km range.

The PX-1000 has dual polarization and in Fig.1 are plotted the long pulse, the fill in pulse, and the compressed pulse. The compressed pulse produces sidelobes in the range weighting function that can contaminate the desired signal. This may be detrimental if the desired signal such as from smoke plumes is weak; the plume starts at the ground and ascends. To detect it as early as possible it is important to scan as close to the ground as possible. But ground produces its own returns. It is possible to have a situation whereby the plume signal is stronger than the ground clutter from the same location. But at closer or farther distances the ground clutter could be much stronger so that its returns through the range sidelobes mask the desired but weaker return from the plume. Another disadvantage of pulse compression is that the long pulse prevents measurement at close range unless it is followed with a short pulse (at a

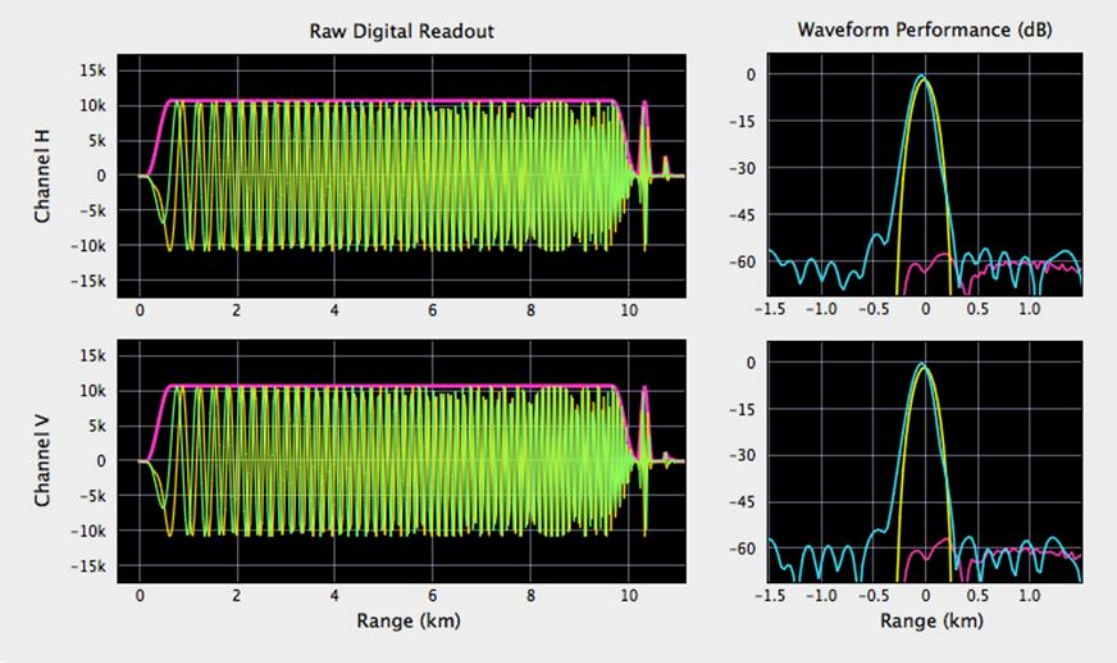

Fig. 1) The long pulse of the PX-1000 radar (3 cm wavelength). The pulse depth is 10 km hence it is not possible to measure returns from this pulse at ranges smaller than 10 km. Therefore a short pulse at a different frequency is sent immediately following the long one and it provides returns to 10 km range. The range weighting functions envelope is depicted by the compressed pulse (blue color). The range weighting function of the short pulse is depicted in yellow and the two range weighting function are fairly well matched within the mainlobe. The range sidelobes of the long pulse are about 60 dB below and the peak but the short pulse has no weighting outside of about 50 m interval. The magenta curve represents the cross polar weighting function, that is caused by coupling between the H and the V signals (Figure courtesy of Dr. Boon Leng, University of Oklahoma).

different frequency). That way the observed range interval is divided into close range (say 10 km sampled with the short pulse) and a long range sampled with the compressed pulse. The transmission between the two intervals creates discontinuities in the polarimetric variables and in the detectability of returns. This is seen in Fig. 2 where a distinct ring at 10 km separate the close region where the short pulses are used from the region beyond where the long pulses produce the return. Note that the polarimetric variables exhibit a change in value (discontinuity) at the 10 km transition. This could be detrimental for classification of the scatterers, i.e., identifying that the return is from a plume.

The detectability is different inside the 10 km range from outside of it and this is illustrated in Fig. 3. A careful look indicates that the 0 to 5 dBZ contour (lightest shade of gray) is just detectable at about 10 to 15 km range which is the beginning of the long pulse domain. The 2 dBZ detectability presented in the Table 1 is within the 0-5 dBZ contour suggested from the visual inspection of the Fig. 3. Closer in (8 to 10 km) the short pulse detectability is 15 to 20 dBZ (blue contour). This agrees with the theoretically predicted value which is about 18 dB worse in the short pulse mode (at 10 km) than it is in the long pulse mode (at 10 km).

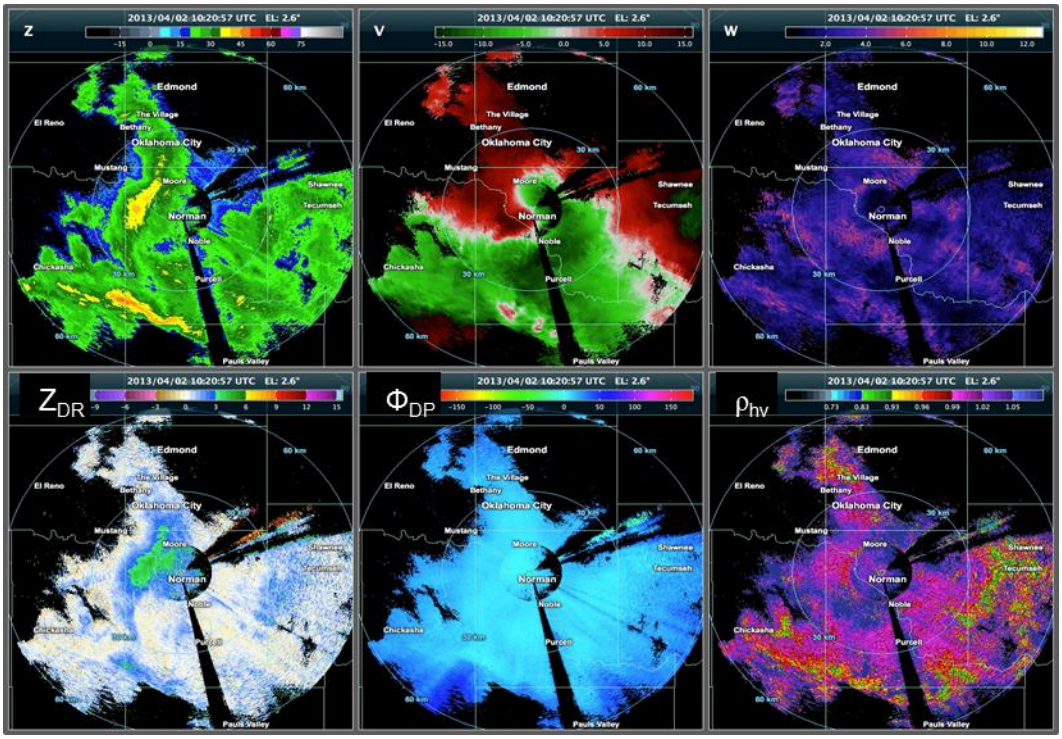

Fig. 2) The fields of reflectivity *Z* (dBZ as indicated by the color bar), Doppler velocity *v* (in m/s as indicated on the color bar), spectrum width *w* (in m/s), differential reflectivity Z_{DR} (dB), differential phase Φ_{DP} (in deg), and correlation coefficient ρ_{hv}. The data were obtained with the PX-1000 radar in Norman OK, on April 2, 2013. (Figure courtesy of Dr. Boon Leng, University of Oklahoma).

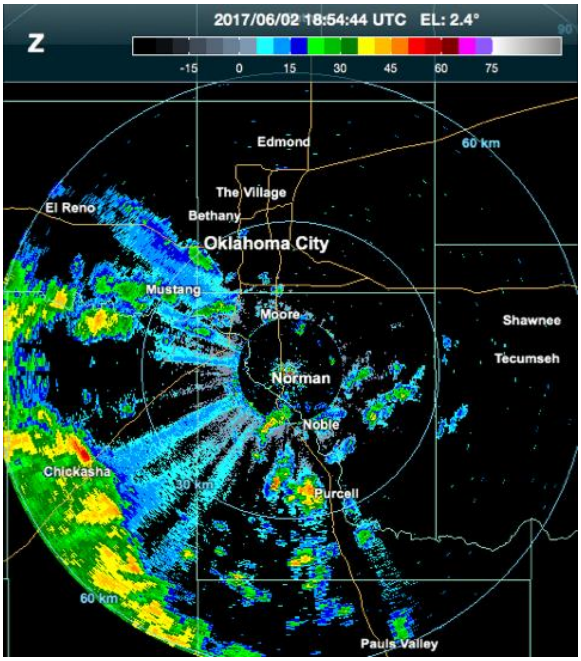

Fig. 3) Reflectivity (in dBZ as indicated by the color bar) obtained with the PX-1000 radar illustrating the increase in detectability slightly farther than the 10 km range. (Figure courtesy of Dr. Boon Leng, University of Oklahoma).

It is apparent that the DOW's detection capability of $Z_{10} = -24$ dBZ is comparable to the WSR-88D's. It is about 4 dB better than the NSSL's dual pol radar (XERES), primarily because it has separate 250 kW transmitter for each polarization whereas the XERES has one transmitter whose power is split into two.

Finally, we present a bit of information about the marine type radars. There is a huge variety of these and it is hard to define a typical one. Therefore, we looked at the recommendation by the International Technical Union (ITU-R M.1313 see the reference) concerning marine type radars. In their table 2 listed are the ranges of values. We choose the favorable ones like the peak power of 50 kW which is about the maximum listed (recommended). The maximum vertical beamwidth is 26 deg, we choose 25 deg (as it is common on marine radars) and a horizontal beamwidth of 1 deg. The gain is 32 dB. If the other parameters are same as on the RaXPol the detectability difference between the RaXPol and the marine radar is $P_{tR} g_R^2 \theta_{1R}^2 / (P_{tM} g_M^2 \theta_{1M} \theta_{2M})$, as can be seen from eq. 1b in (Zrnic et al. 2017). The superscripts *R, M* stand for RaXPol and Marine radars. With these most favorable values to the marine radar its detectability (Z_{10}) is 7 dB lower than the RaXPol's. But that assumes the beam is filled with the plume, which will not be the case. The 25 deg elevation at 10 km corresponds to the height of more than 4 km. If the plume extends few hundred meters above ground the additional loss due to incomplete beam filling would be more than 10 dB. For these reasons we submit that the most powerful marine radars are not suitable for detection of plume at ranges beyond about 1 km.

The attenuation by rain is the most detrimental aspect for operational detection of plumes with X band radars because such detections must be made in all types of weather. The attenuation has been quantified by Zrnic et al. (2017). Herein we present a couple of cases which were observed by the X band and S band (WSR-88D) radars.

In Fig. 4 are the observations made by the WSR-88D located in Amarillo TX and the UMass XPol mobile radar (Table 1). At many places a complete loss of signal occurs after less than 10 km of propagation through the heavy rain.

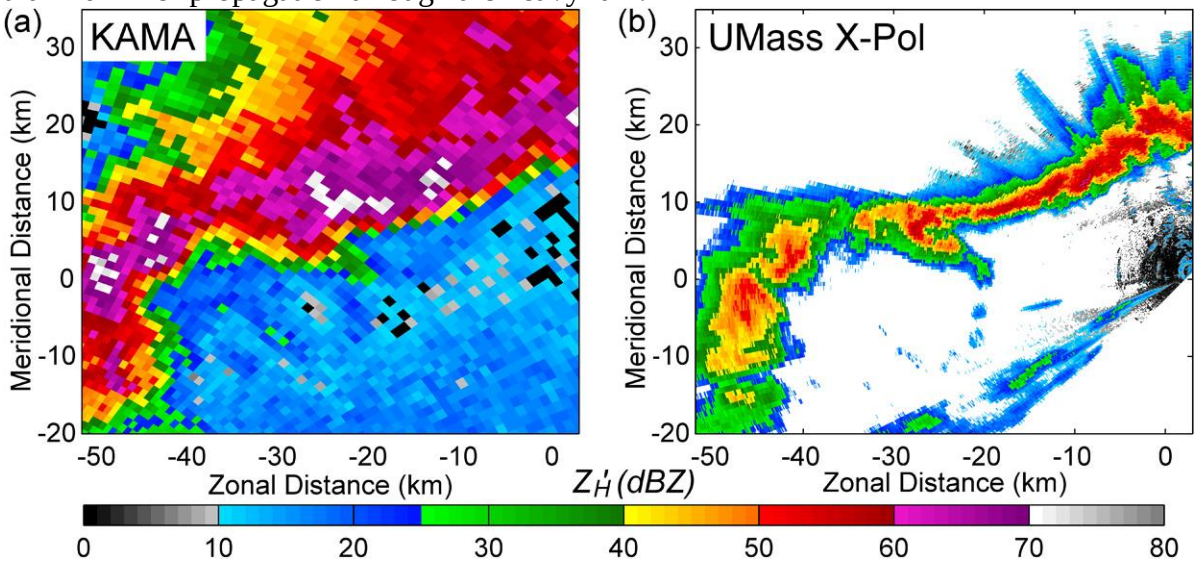

Fig. 4) Reflectivity fields a) from the KAMA (Amarillo, TX) WSR-88D radar. b) From the UMass XPol radar ((.41 GHz). 21May 2007. Figure courtesy of J. Snyder (adapted from Snyder et al. 2010).

The case in Fig. 5 is from Oklahoma and it shows the reflectivity factor *Z*, the differential

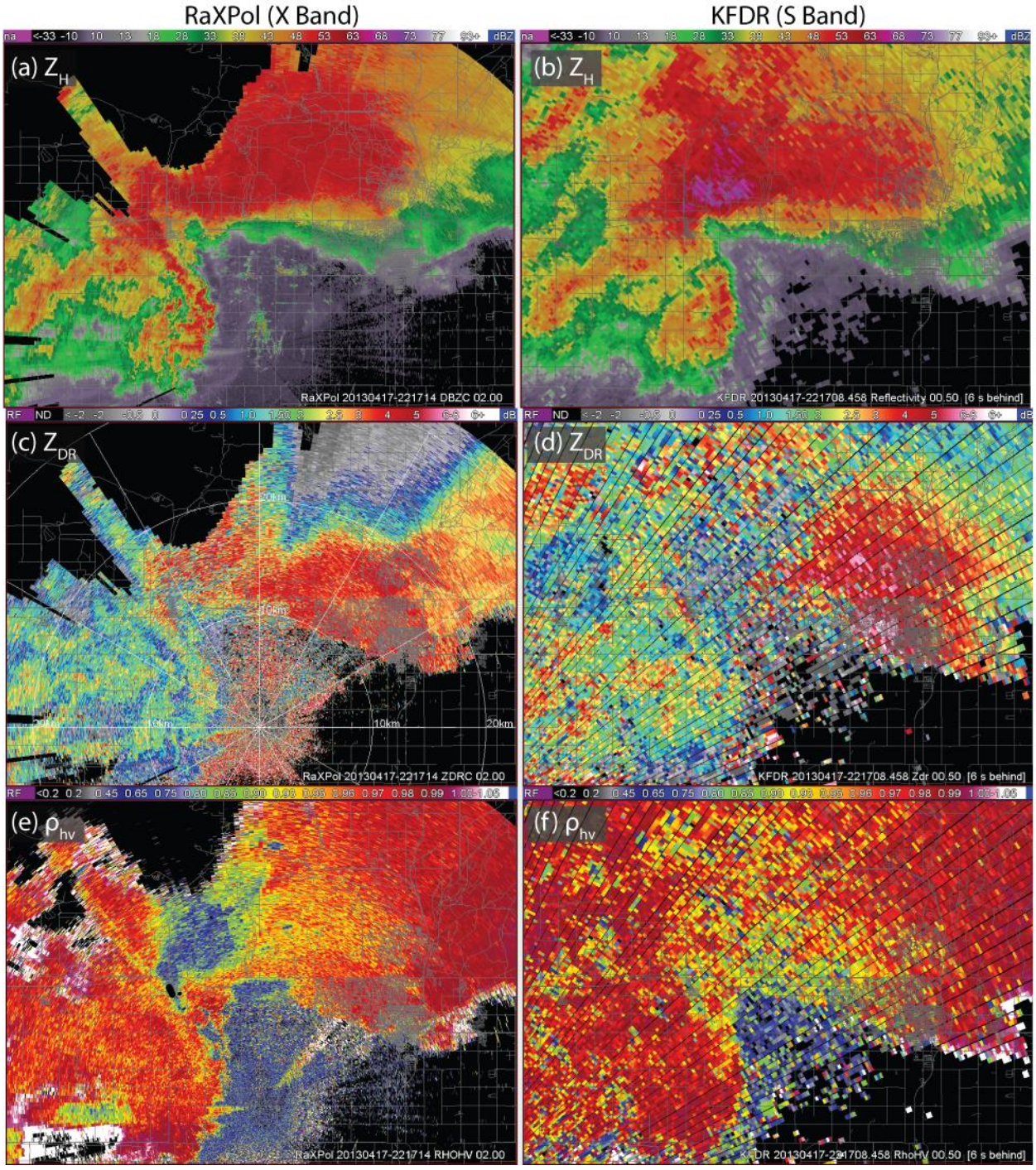

Fig. 5) Fields of polarimetric variables. On the left are the polarimetric variables obtained with the RaXPol radar (Table 1 has the characteristics). On the right are the same variables obtained with the WSR=88D (KFDR) in Fredrik OK. Figure courtesy of J. Snyder (adapted from Snyder et al. 2010).

reflectivity Z_{DR}, and the correlation coefficient ρ_{hv} measured with the RaXPol (Table 1) and the WSR-88D (Enid OK). General agreement between Z_{DR} in the NE quadrant is evident as is the agreement of the low ρ_{hv} in the clear air region (insects likely) in the SE quadrant. Otherwise the effects of propagation are clearly visible in the RaxPol data as negative gradients of Z_{DR} along the beam (NE quadrant) and attenuation in the NW quadrant. The finger like protrusion close to 330^o with respect to the RaXPol is caused by the three body scattering mechanism (Zrnic 1987). Through the heavy precipitation along about 350^o of the RaXPol the signal is heavily attenuated and vanishes beyond about 8 km.

In Fig. 6 are the fields of the radar variables obtained with the NSSL's mobile radar

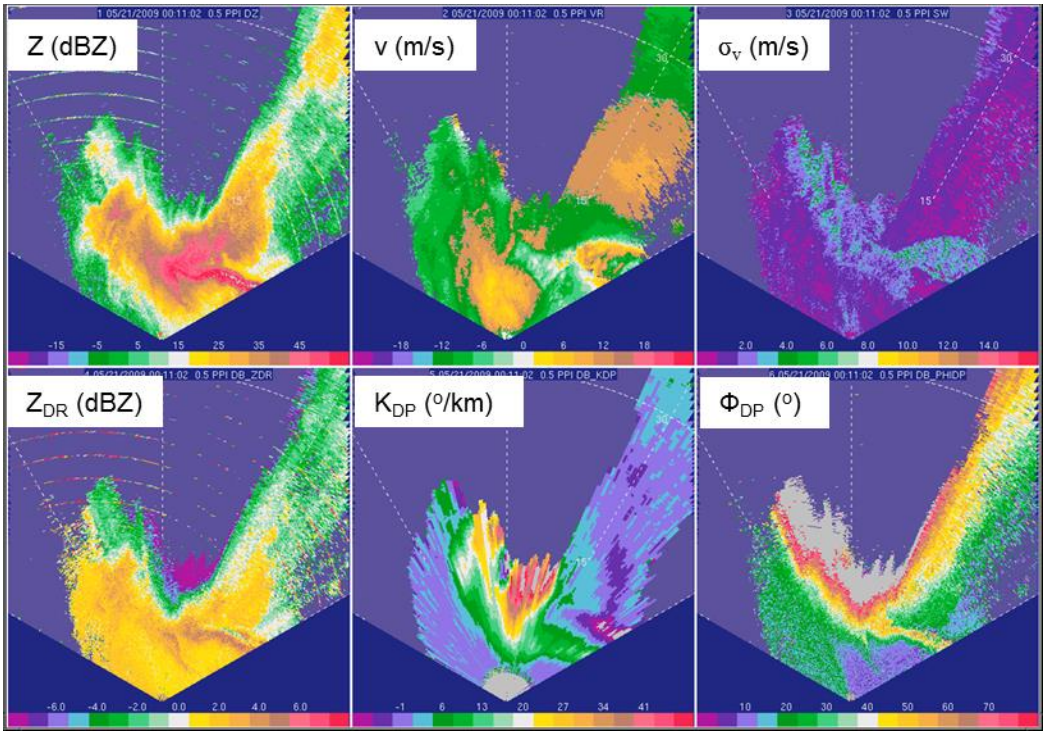

Fig. 6) Fields of radar variables. Reflectivity is denoted with *Z*, Doppler velocity is indicated with *v*, spectrum width with σ_v, differential reflectivity with Z_{DR}, specific differential phase with K_{DP} and total differential phase with Φ_{DP}. The range mark is at 30 km. Data were obtained on May, 21, 2009 with the NSSL's mobile radar (XERES, 3 cm wavelength, table 1).

(XEREX table 1). The purpose is to illustrate the quality and capability of this radar because it can be used at a modest cost for field experiments. Again a significant loss caused by precipitation is evident as a notch between about 350 deg azimuth and 40 deg. The heavy attenuation can be quantified by the large values of the specific differential phase (K_{DP} up to 40 deg km^{-1}) as well as the increase of total differential phase Φ_{DP} with range from about 6 deg (green color) to about 90 deg (red color) over a distance of about 7 km; farther in range the signal vanishes. Note that the Z_{DR} is mainly about 2 dB (yellow contour) but occasionally reaches 4 dB (brown streaks) indicating large drops (possibly containing ice cores). It is significant that the Z_{DR} becomes negative in the notch reaching values smaller than – 6 dB (purple reddish color). These large negative values are cause by differential attenuation. The horizontally polarized signal is attenuated at least 6 dB more than the vertically polarized one.

Discussion 1: Some of the existing X band radars have detection capability similar to the ones on the WSR-88D or TDWR. Thus, in clear air these radars have an advantage because for a given reflectivity of a plume the plume signal to ground clutter ratio is larger at the shorter wavelength as the clutter cross section per unit area (in the 3 to 10 cm range) is roughly proportional to wavelength λ^{-1} (Billingsley 2002). The cross section of Rayleigh scatterers is proportional to λ^{-4}. Thus under the same conditions (plume reflectivity, clutter, beamwidths, pulse widths, elevation, etc.) the signal to clutter ratio at the 3 cm is better by a factor of $(10/3)^3$ compared to the 10 cm wavelength. This is a definite advantage for measurements of plumes because these are close to the ground and produce weak returns so that any enhancement against clutter can make a difference between detection and misses. The mobility of the X band radars facilitates research experiments, for example measurements of artificially generated plumes because both the radar and the experiment location can be chosen to optimize detection. This is more constrained for fixed radars because only the location of the experiment can be changed limiting the freedoms of choice. The X band radars with pulse compression can be used for research experiments as the positions of the radar and the experiment can be adjusted to optimize the sensitivity and avoid the transmission between the short and long pulse domain. But for operational detection of plumes pulse compression is not recommended. Nonetheless the biggest obstacle to the X band radars is attenuation by precipitation.

b) *Radars with wavelength in the mm range*

MilliMeter Cloud Radars (MMCR) are typically used for cloud studies in a vertically pointing mode. The DOE at Atmospheric Radiation Measuring sites has such radars (MMCR-8 in table 1) and NASA's Cloud System Radar (CSR[8] in table 1) is also ground based. MMCR are often use on airplanes (NASA's CSR[9] in table 1) or even satellite. It can be seen in Table 1 that the 8 mm (MMCR-8) and the 3 mm (CRS[10]) radars have very high detection capability. But what the table does not tell is the attenuation in air or in precipitation. In humid air the attenuation of 8 mm EM waves is 1 dB km^{-1} and of the 3 mm waves it is 2.5 dB km^{-1}. Thus, these radars are not suitable for reliable ground based surveillance. They could detect plumes if flown on airplanes and pointed down; this, however, is not practical for routine operational application.

Table 3: CPR parameters

Nominal Frequency	94 GHz
Pulse Width	3.3 µsec
PRF	4300 Hz
Minimum Detectable Z[1]	< -29 dBZ
Antenna Size	1.85 m
Integration Time	0.16 s
Nadir Angle	0.16°
Vertical Resolution	500 m
Cross-track Resolution	1.4 km
Along-track Resolution[2]	1.7 km
Altitude	710 km

[1)] Equivalent radar reflectivity that gives a mea n power equal to the standard deviation after integration and noise subtraction.
[2)] The along-track resolution is based on averaging the instantaneous footprint over the integration time. Based on purely geometric arguments, the along-track resolution would be approximately 2.5 km. However, a more rigorous convolution calculation gives an along-track resolution of 1.7 km, as shown in the table.

The last MMCR radar listed in the Table 1 is the satellite born Cloud Profiling Radar. Its published parameters are in the Table 2. The detectability in Table 1 is obtained indirectly from the Table 3 and appropriate relations between the SNR and the variance reduction of power estimates that occurs if M samples are averaged (M=0.16*4300=688), see Melnikov (2004 eq. A10).

Note that the resolution is very poor for early detection of plumes which initially have a very small volume. The minimum detectable Z is for scatterers that fill uniformly the whole resolution volume therefore the actual detectability of plumes from this radar would be much lower. The reduction is 10 log[.5*1.4*1.7/Volume (km^3)], where the plume's total Volume is in km^3. As example assume that a plume with the reflectivity of – 3dBZ fills a volume V (see section 3 for values of Z in plumes). The difference – 3dBZ –(-33 dBZ) = 30 dB. This is a factor of 1000, therefore to be detected the plume volume must fill at least .5*1.4*1.7/1000 km^3 which is a cube of about 105 m on the side.

Discussion 2: Millimeter wavelength radars are not good candidates for detection of plumes primarily because of the large attenuation in precipitation and even in humid air. For research purposes these radars could observe plumes by being flown over on airplanes.

3. Measurements

A brief discussion of polarimetric variables is present to set the stage of the section on data analysis.

a) Polarimetric variables

The WSR-88D as well as most of the polarimetric weather radars operate in the simultaneous mode whereby the horizontally and vertically polarized waves are transmitted and receive simultaneously (SHV mode). Thus, the transmitted wave has an elliptic polarization with known horizontal and vertical components (but unknown phase between these two). On reception the two components are separated at the antenna and processed through two receivers to produce four polarimetric variables. These are the equivalent reflectivity factor Z_h at horizontal polarization, the differential reflectivity, the correlation copolar coefficient, and the differential phase.

Differential reflectivity is defined as

$$Z_{DR}=10 \log (P_h/P_v) = Z_h-Z_v, \qquad (1)$$

where P_h, P_v are the returned powers at horizontal, vertical polarizations and Z_v is the equivalent reflectivity factor at vertical polarization. Because (1) is a ratio it does not depend on the concentration of particles in the resolution volume (the concentration cancels out). Rather it depends on the ratio of weighted reflectivities by their pdf in the horizontal direction to the one in the vertical direction. In that sense Z_{DR} contains information about the "average" aspect ratio of the ensemble of particles.

Correlation coefficient is defined as

$$\rho_{hv} = \frac{V_h^* V_v}{\sqrt{P_h P_v}}, \qquad (2)$$

where the voltages V_h, V_v are in the channel for horizontal, vertical polarization. The * indicates conjugate. Therefore, ρ_{hv} is a complex number. In the sequel we use notation (2) to indicate the

magnitude of this complex number. The correlation coefficient indicates the diversity in shapes of the particles, as well as wobbling, and misalignment. It is a very good indicator of precipitation most of which produce values larger than about 0.97. Wet snow and hail lower the correlation to about 0.9; non-meteorological scatterers have values significantly lower than 0.9.

Differential phase Φ_{DP} is the argument of (2) it quantifies the phase difference between the returned polarized signals.

The four polarimetric variables are available as level 2 data on the WSR-88D radars. In addition, the range derivative $d(\Phi_{DP})/dr$ constitutes the specific differential phase and is used for quantitative rainfall measurements. These variables can also be computed from the level 1 data (time series) if a recorder is attached to collect such data.

For classification of returned signals the four polarimetric variables are used. The textures of Z, Z_{DR}, and ρ_{hv} can also be useful for classifying echo types. A description of the classification algorithms (developed by NSSL) on the WSR-88D is contained in Park et al. (2009). More recently Krause (2017) has proposed an algorithm to separate non-meteorological scatterers from the meteorological ones. This algorithm is on the Radar Product Generator and its main purpose is to eliminate false detections of specific differential phase (K_{DP}). It is applied before K_{DP} is computed (from total differential phase Φ_{DP}) and its result determines if K_{DP} will be computed and used for rainfall accumulation (in case of meteorological class) or censored.

Non meteorological returns come from biological scatterers (insects, birds, bats), ground (grass, forests, buildings), ocean, plumes (smoke, volcanic ash, explosion debris), and vehicles (trains, automobiles, airplanes): Lakshmanan et al. (2015) succinctly analyze the relative importance of the polarimetric variables for discrimination between weather and non-weather returns.

Discussion 3. The returns from plumes are currently lumped together into a category of non-meteorological signals (complement of the met-signal category). There has been no systematic study to determine the polarimetric signatures of various plume types. Such study is proposed for the near future so that these phenomena can be early detected and tracked. To quantify returns from plumes histograms of the polarimetric variables and scattergrams of two polarimetric variables at a time are needed. These should be obtained from a wide variety of plume types and in a variety of environmental conditions.

b) *Data analysis*

An analysis of a wild fire case is presented to illustrate the capabilities and issues. The Little Bear fire occurred in New Mexico near Ruidoso on June 8, 2012 and was started by lightning strike. The fire quickly progressed, burned 44 330 acres and consumed 254 buildings. Fire progression over one-hour time is mapped in Fig. 7, the corresponding satellite images are in Fig. 8 and fields of polarimetric variables are in Figs. 9, 10 and 11. These fields were

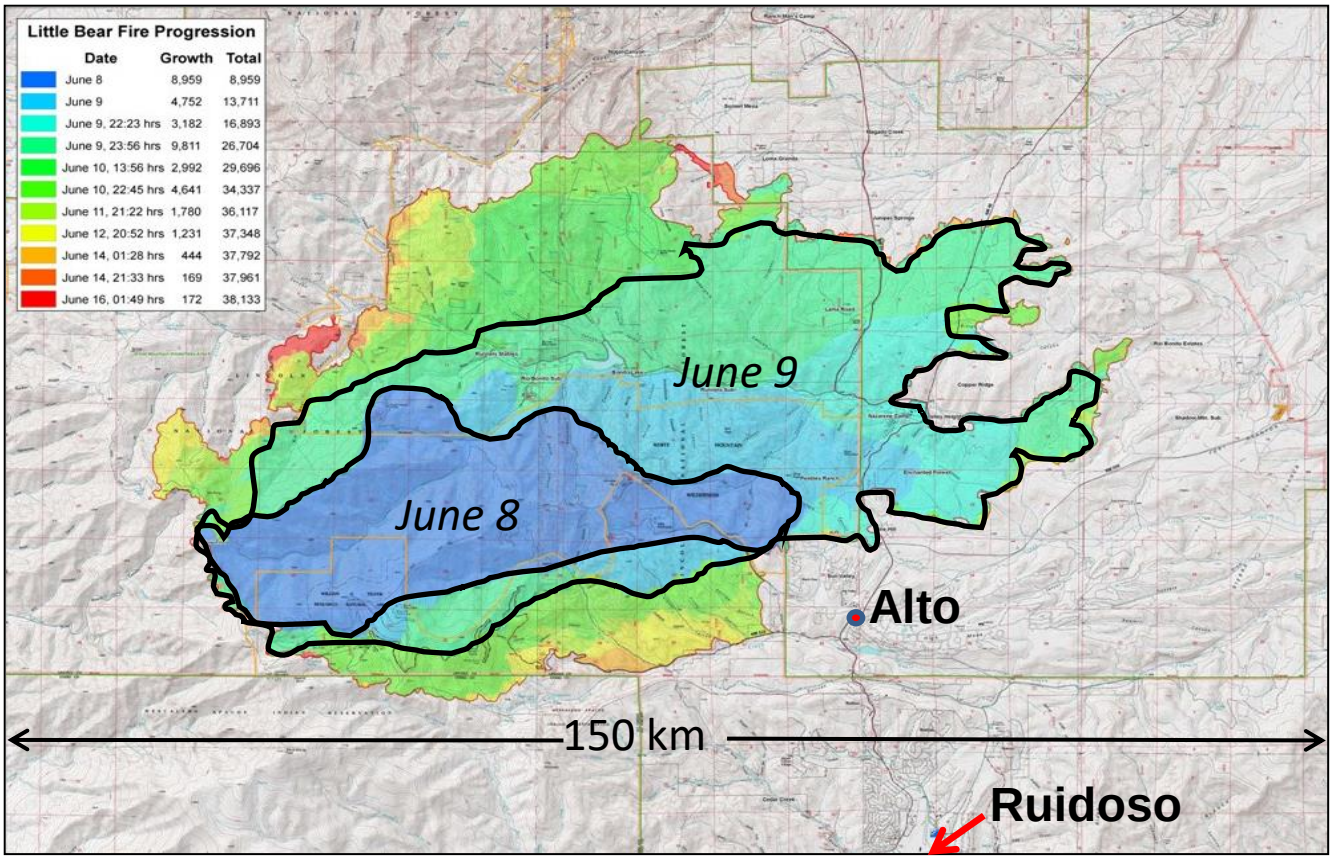

Fig. 7 Map of Little Bear fire progression. New Mexico June 2012.

obtained by the Holloman weather radar (WSR-88D designated as KHDX).

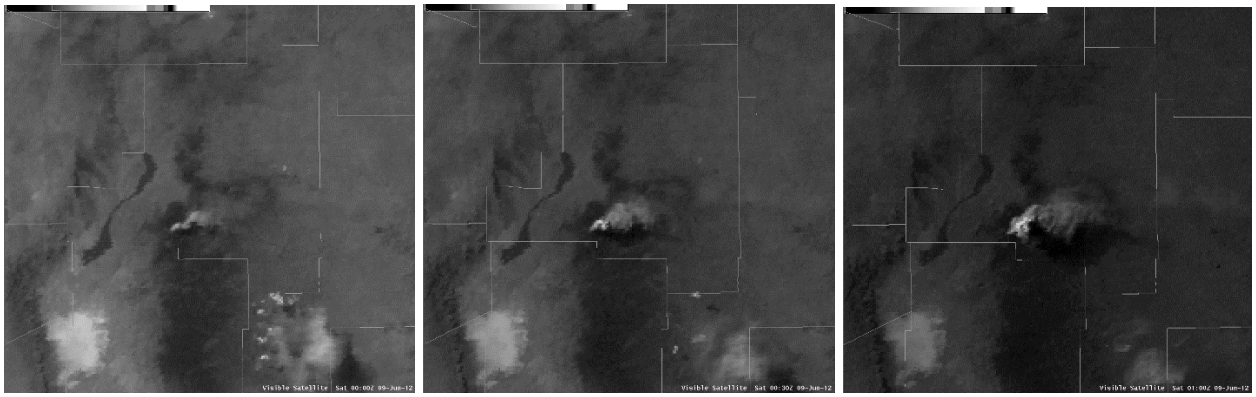

6 pm 6:30 pm 7 pm

Fig. 8. Satellite image of the Little Bear fire at three consecutive times on June 8, 2012.

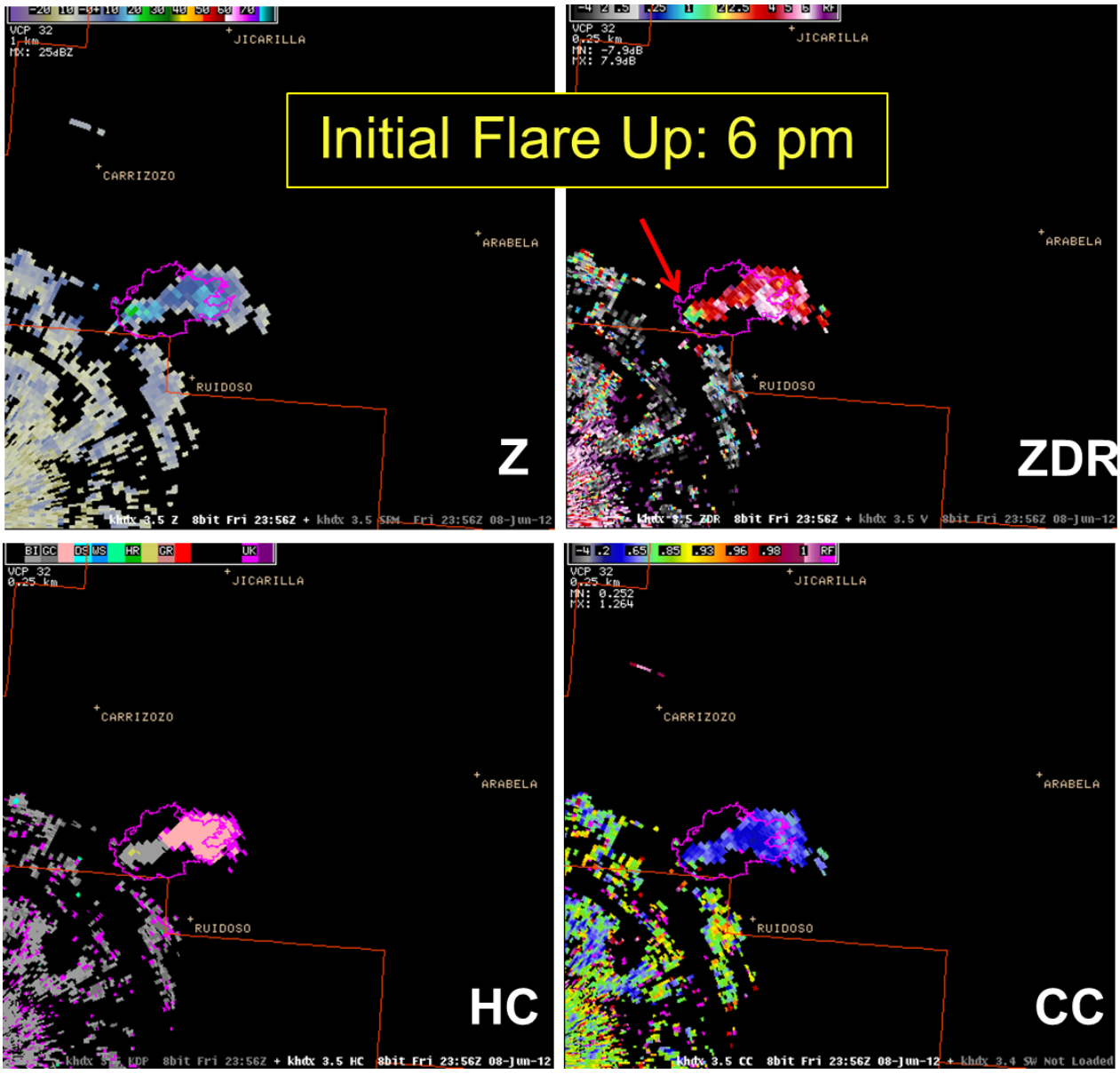

Fig. 9. Fields of Reflectivity *Z*, differential reflectivity Z_{DR}, and correlation coefficient ρ_{hv} obtained with the Holloman (Air Force Base) radar on June 8, 2012. This image corresponds to the satellite imager (leftmost in Fig. 8).

Noteworthy are the relatively high values (~ 30 dBZ) of the reflectivity field. The highest values are at the SW part which is the location of intense burning. The fire generated updraft lofts debris which in the updraft has high concentration and might contain largest scatterers (possibly carbonated grass, or leaves etc.). The relatively low values of Z_{DR} (about 1 dB) indicate that the particles tend to be horizontally oriented but are likely wobbling, lowering the effective Z_{DR}. Further downwind (to the NE) there is a secondary maximum of *Z* coincident with very large

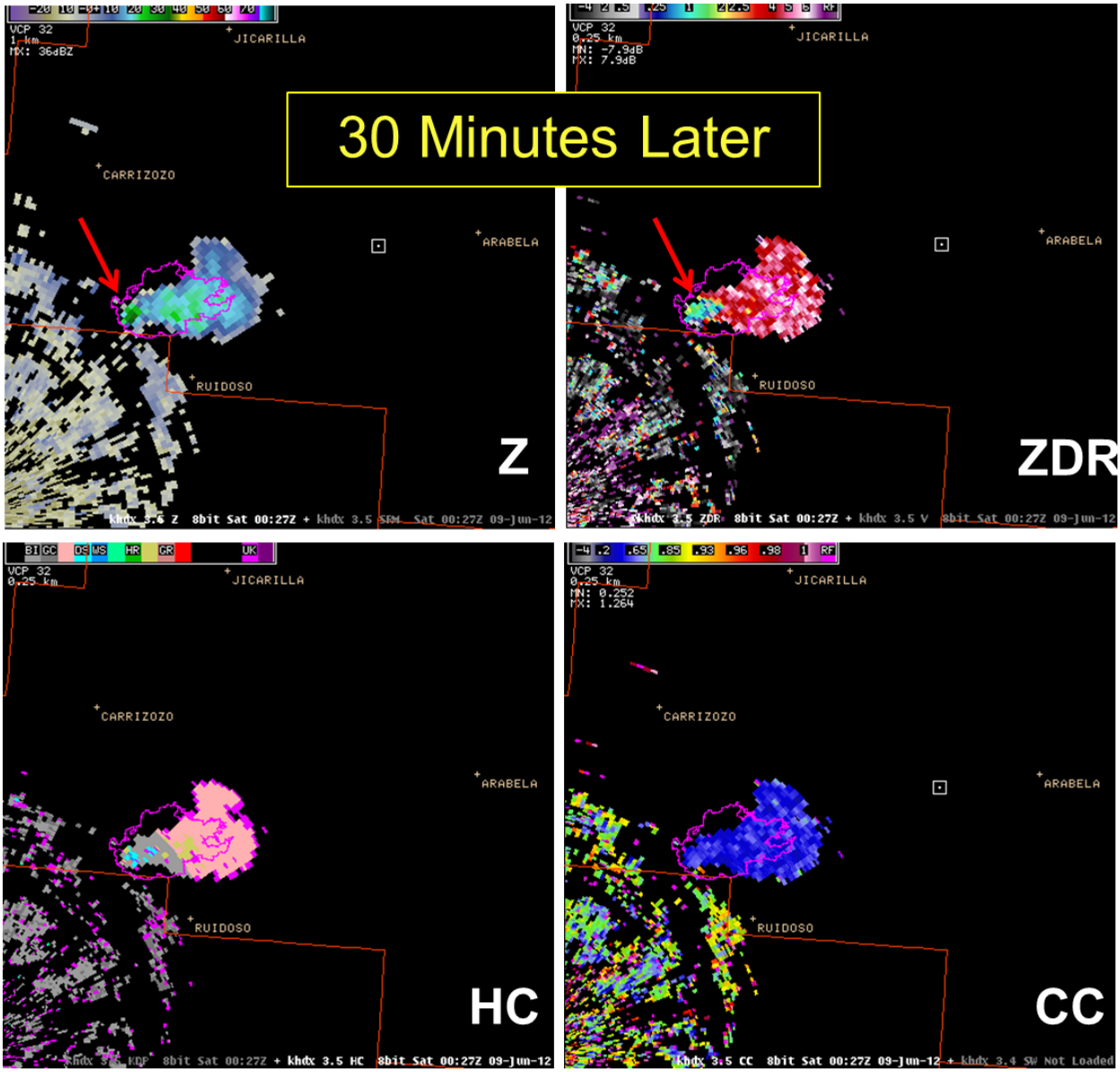

Fig. 10. Fields of Reflectivity *Z*, differential reflectivity Z_{DR}, and correlation coefficient ρ_{hv} obtained with the Holloman (Air Force Base) radar on June 8, 2012. This image corresponds to the satellite imager (middle in Fig. 8).

differential reflectivity. We do not know the exact composition of scatterers but speculate that either the burned debris is getting oriented away from the updraft or smoke particles act as condensation nuclei which caused crystal formation (needles and plates) so these show as increased reflectivity and differential reflectivity. In either case the low values of the correlation coefficient (0.6) suggests that there is significant flutter (random canting) of the particles. The hydrometeor classification algorithm was applied (by the weather service) to these data but the results are not correct. At the updraft location the majority of pixels are classified as "biological scatterers" which clearly these are not. Some scatterers (pink category) are classified as horizontally oriented crystals (there might be some there), and we also see "big drops" which are

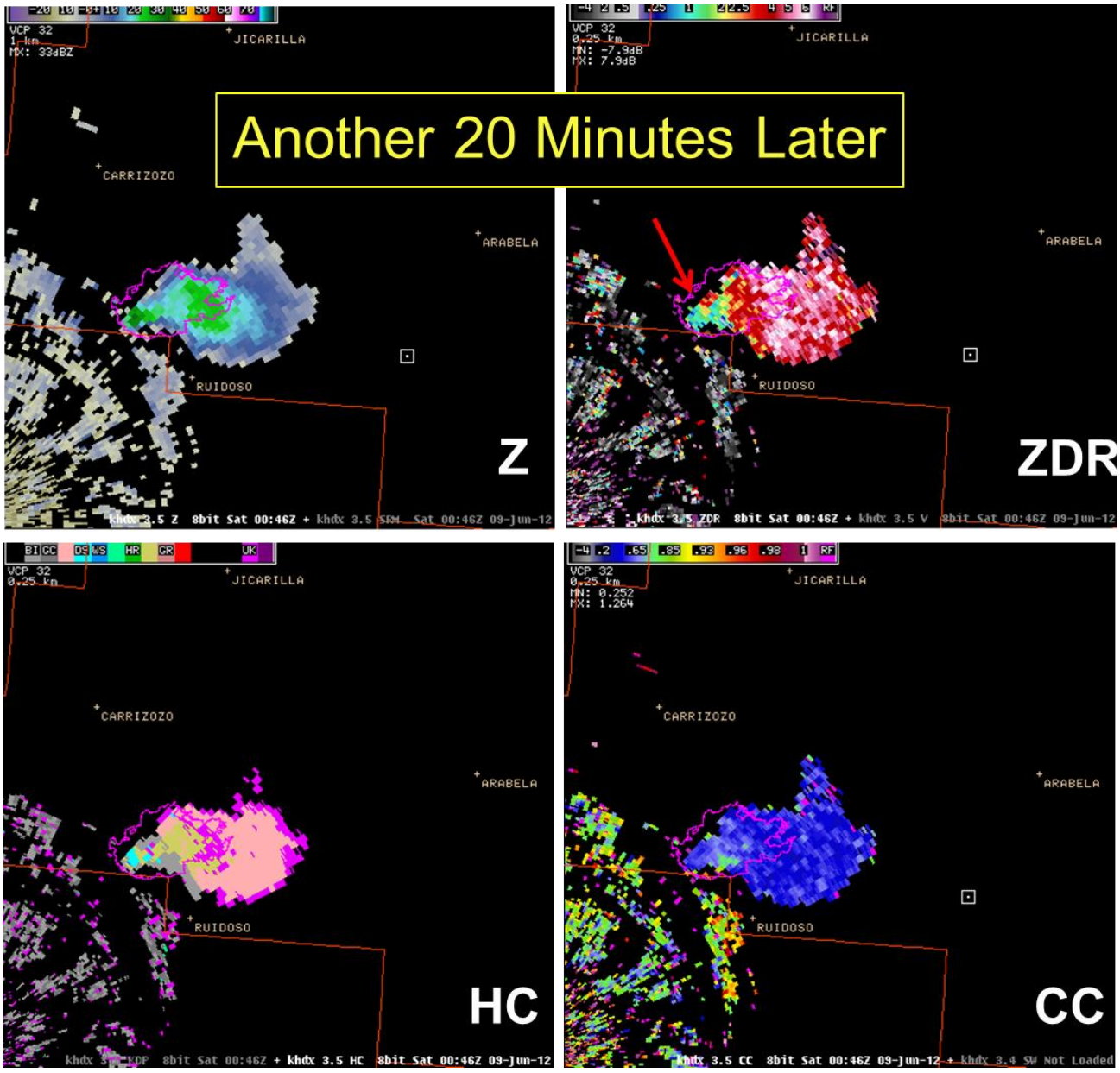

Fig. 11. Fields of Reflectivity Z, differential reflectivity Z_{DR}, and correlation coefficient ρ_{hv} obtained with the Holloman (Air Force Base) radar on June 8, 2012. This image corresponds to the satellite imager (rightmost in Fig. 8).

doubtful. The classification algorithm has not been adjusted to discriminate smoke plumes. To achieve such discrimination much work needs to be done.

In Fig. 12 the polarimetric fields in the fire areas are encompassed with polygons. Histograms of the data from these polygons (Fig. 13), indicate the mean values and spread for this particular fire. The mean values are about 12 dBZ reflectivity, 4 dB differential reflectivity, and 0.55 correlation coefficient. We have plotted also the total differential phase and its mean value of about 60° represents the system differential phase; that is, the differential phase encountered in the transmission chain and reception chain. The radial velocity v_r of about 6 m s^{-1}

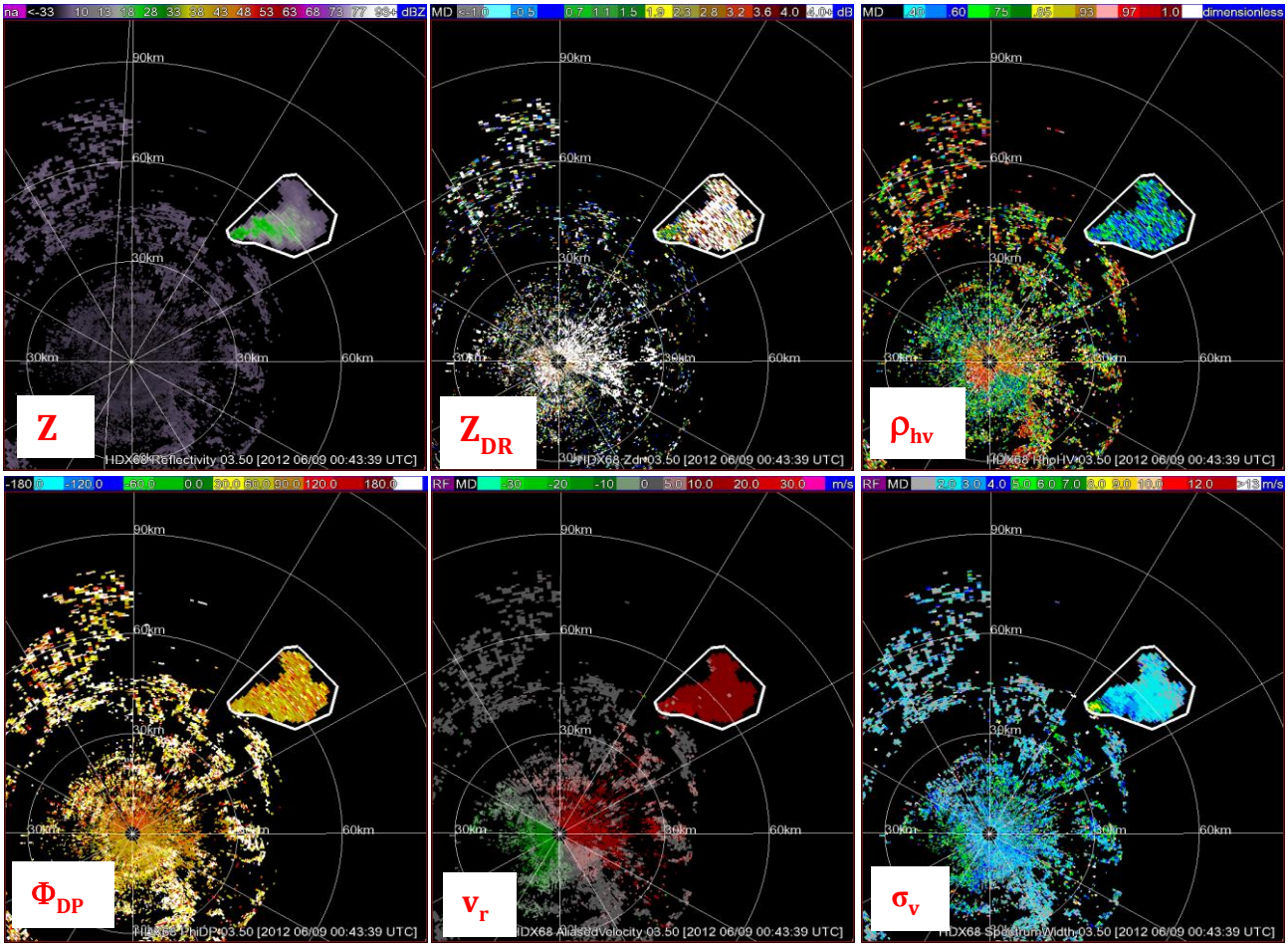

Fig. 12. Polygons encompassing the polarimetric variables of the smoke area.

represents the advection component, and the spectrum width σ_v values up to 3 m s^{-1} indicate that turbulence is present. Scattergrams of Z, Z_{DR} and Z, ρ_{hv} (Fig. 14) are contained within

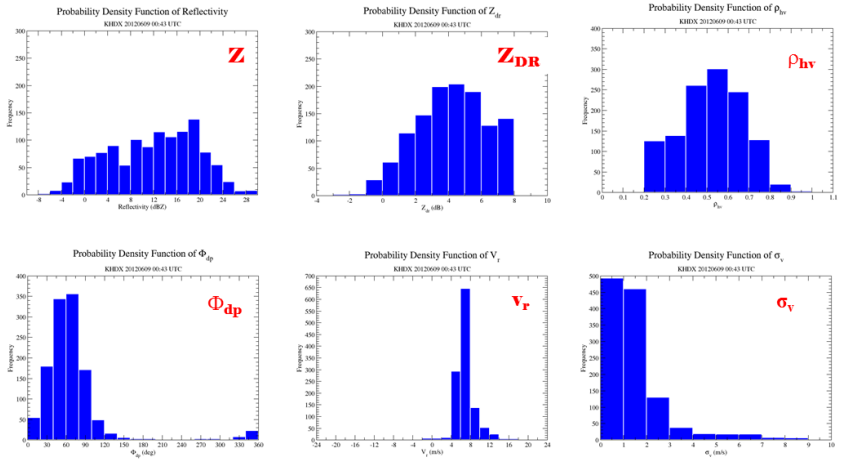

Fig. 13. Histograms of the polarimetric variable within the polygons in Fig. 12.

approximately rectangular domains suggesting that the variables are independent. Hence for fuzzy logic type classification the one dimensional membership functions (at least for these variables) would suffice. For example the membership function for Z would have values of 1 between 0 and 25 dBZ and could taper (decrease) linearly to 0 at higher and lower *Z* values. The membership function for Z_{DR} could be one between 0 and 8 dB, however we alert the reader that the value of 8 dB is the maximum that is currently possible to record on the WSR-88D. Plans are to extend the maximum values to over 10 dB. The membership function for the correlation coefficient could have a value of one between about 0.2 and 0.8. It appears that the minimum possible is 0.2 dB.

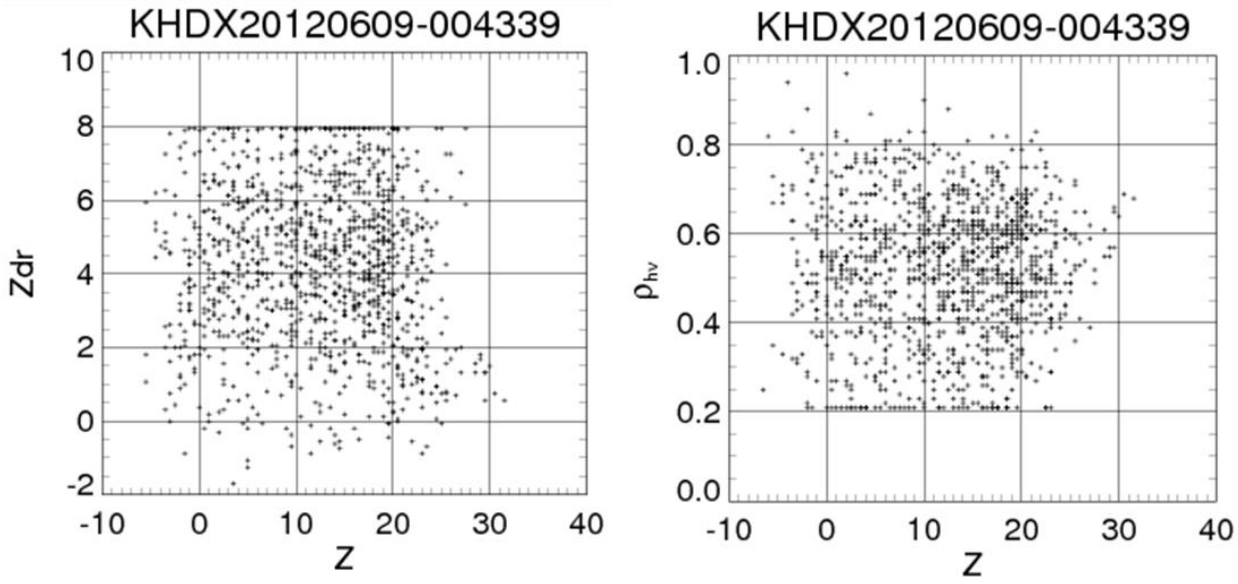

Fig. 14. Scattergrams of the polarimetric variables within the polygon in Fig. 12.

c) *Fireworks experiment*

An experiment was conducted on July 4, 2017 in Norman OK. The purpose was to observe and document the radar return from the fireworks at the Reeve Park in Norman. The map with the location of radars during this experiment is in Fig. 15. The TDWR radar is the one serving the Will Rogers airport in Oklahoma City. It is located at 11.25 km from the Reeve Park where fireworks are held every Fourth of July. We thus decided to take the 3 cm wavelength NSSL radar (XEREX) and locate it about 1.5 km south of the Park and to also bring a video camera for visual confirmation of the events. We planned using the KOUN radar (the NSSL's WSR-88D at about 6 km from the Park) to collect polarimetric data at the 10 cm wavelength. It turned out that the radar experienced a technical issue hence we were not able to use it on that day. We also glanced at the KTLX (operational WSR-88D) radar but did not see obvious returns from the fireworks. We intend to look at the data from the KTLX as well the KCRI, the radar 200 m away from the KOUN, in more details later.

We collected data with the 3 cm polarimetric radar starting at about 2^o elevation and ending close to 10^o. The sector scans were about 35^o. The pulse repetition time was 1 ms, 32 samples were taken per one degree in azimuth so that the rotation rate was about 31 ^{o} s^{-1}. The event lasted about 15 min and we collected the data throughout it. Quick assessment and analysis follows.

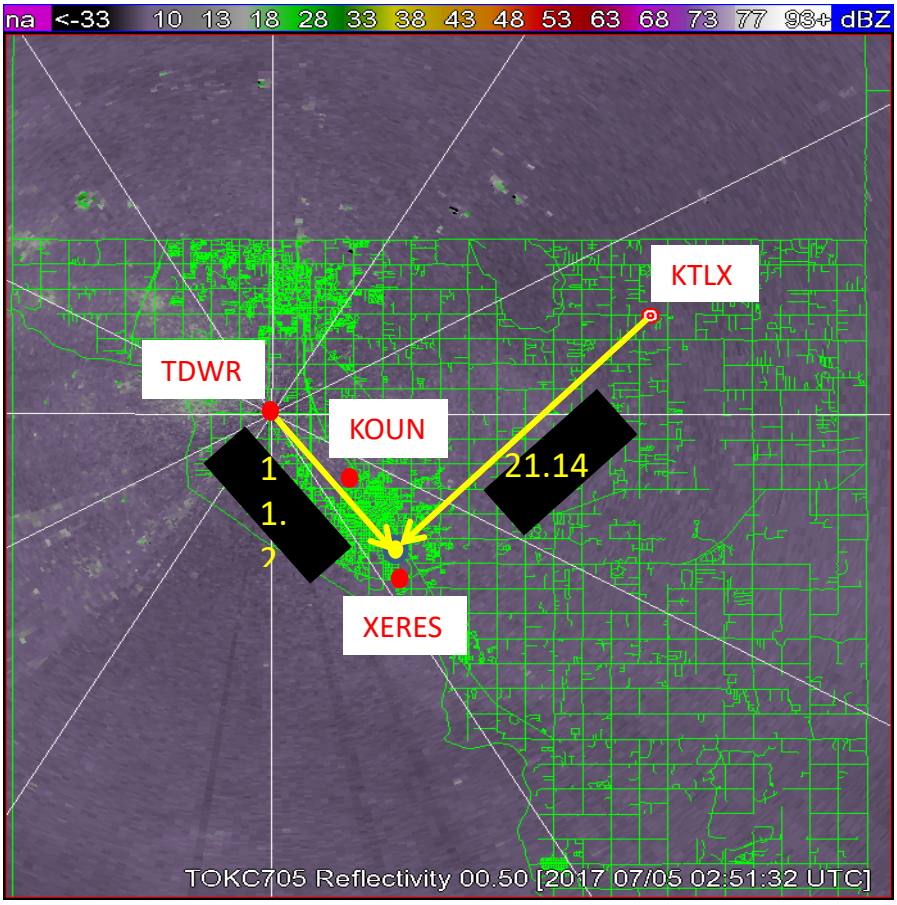

Fig. 15. Location of radars during the experiment of July 4, 2017 in Norman OK. Location of the Reeve Park is indicated with the yellow dot.

The reflectivity at 9.85° elevation (Fig. 16) shows some returns mainly from insects and close in from the ground. The height above ground at 1.5 km range at this elevation is about 250 m and the fireworks did not exceed 200 m hence there is no evidence in Fig. 16 of smoke or debris. The background reflectivity is less than about – 6 dBZ. Seven seconds later at the 3.83° elevation (height above ground is 100 m) there is clear evidence of an increase in reflectivity with the maximum between 22 and 26 dBZ in the patch centered at about 1 km North from the radar. The patch persists in consecutive scans and coincides with the location where the fireworks were lunched. Throughout the event the patch intensified and decayed but did not exceed 26 dBZ in reflectivity. New maxima formed and drifted with the wind. The highest elevation at which we detected faint presence of firework signature was 8.8° corresponding to beam center at about 230 m above ground. The reflectivity factor at this height was less than 10 dBZ suggesting that the fireworks were in the lower part of the beam. Rough estimate is that the bunch of scatterers contributing to the return was at about 200 m above ground. This is estimated from maximum reflectivity of 26 dBZ at beam center (at lower elevations) minus the 10 dBZ at the lower part of the beam (at the elevation of 8.8°). If the 16 dB difference is due solely to the antenna pattern the scatterers would be about 0.8° away from beam center, i.e., at about 8° which

puts them at 200 m above ground. Only on few occasions did we see echoes at such high altitude. The strongest returns were mostly at about 100 m above ground.

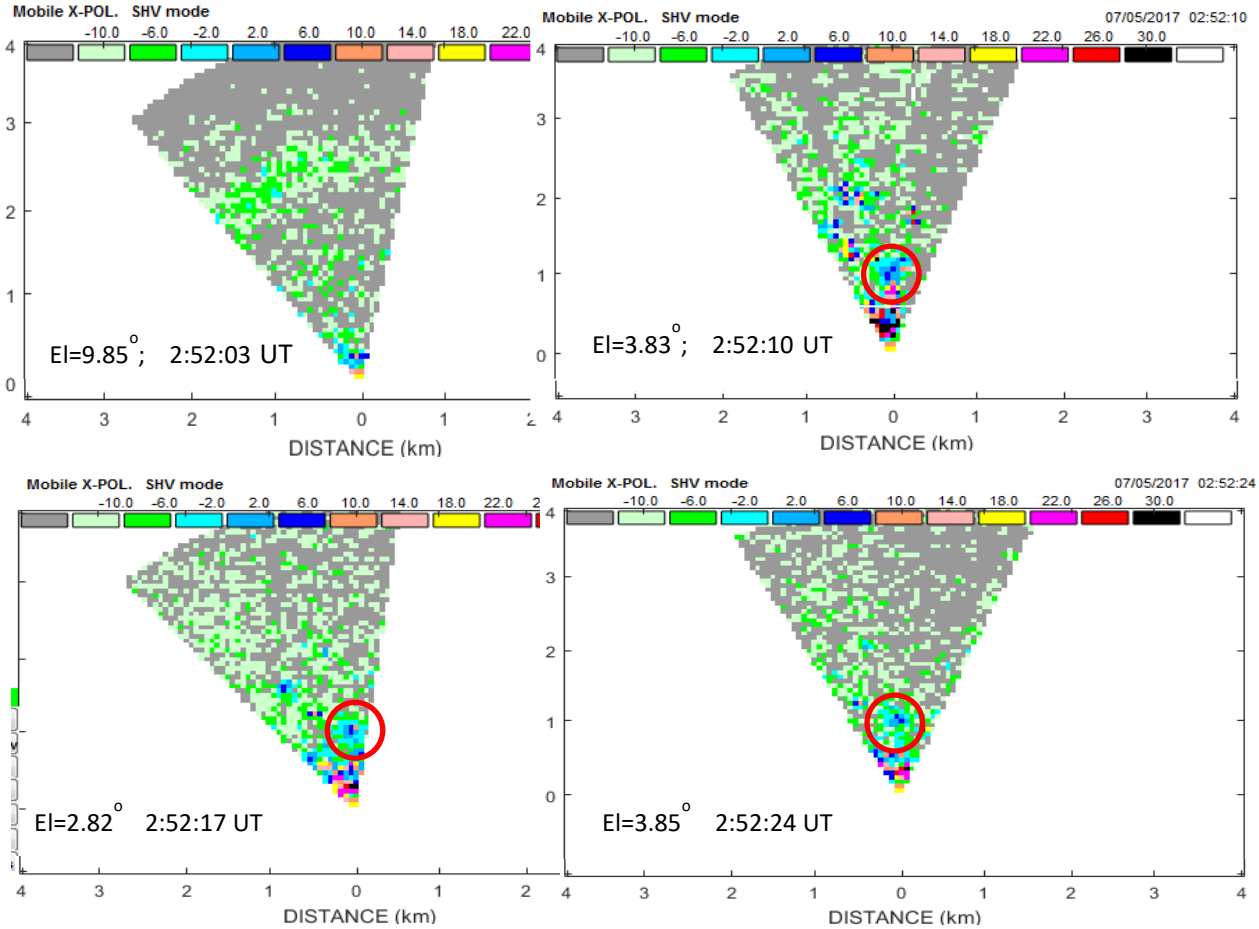

Fig. 16. Reflectivity obtained on July 4, 2017 (July 5 UTC) with the XERES (3 cm wavelength) dual polarization radar. The red circle indicates fireworks signal. Elevation angles and times (universal time is 5 hours ahead of the local time).

The polarimetric variables Z_{DR} and ρ_{hv} have no discernible features associated with the fireworks (Fig. 17). This is likely cause by the presence of insects which produce similar values to the ones from the fireworks.

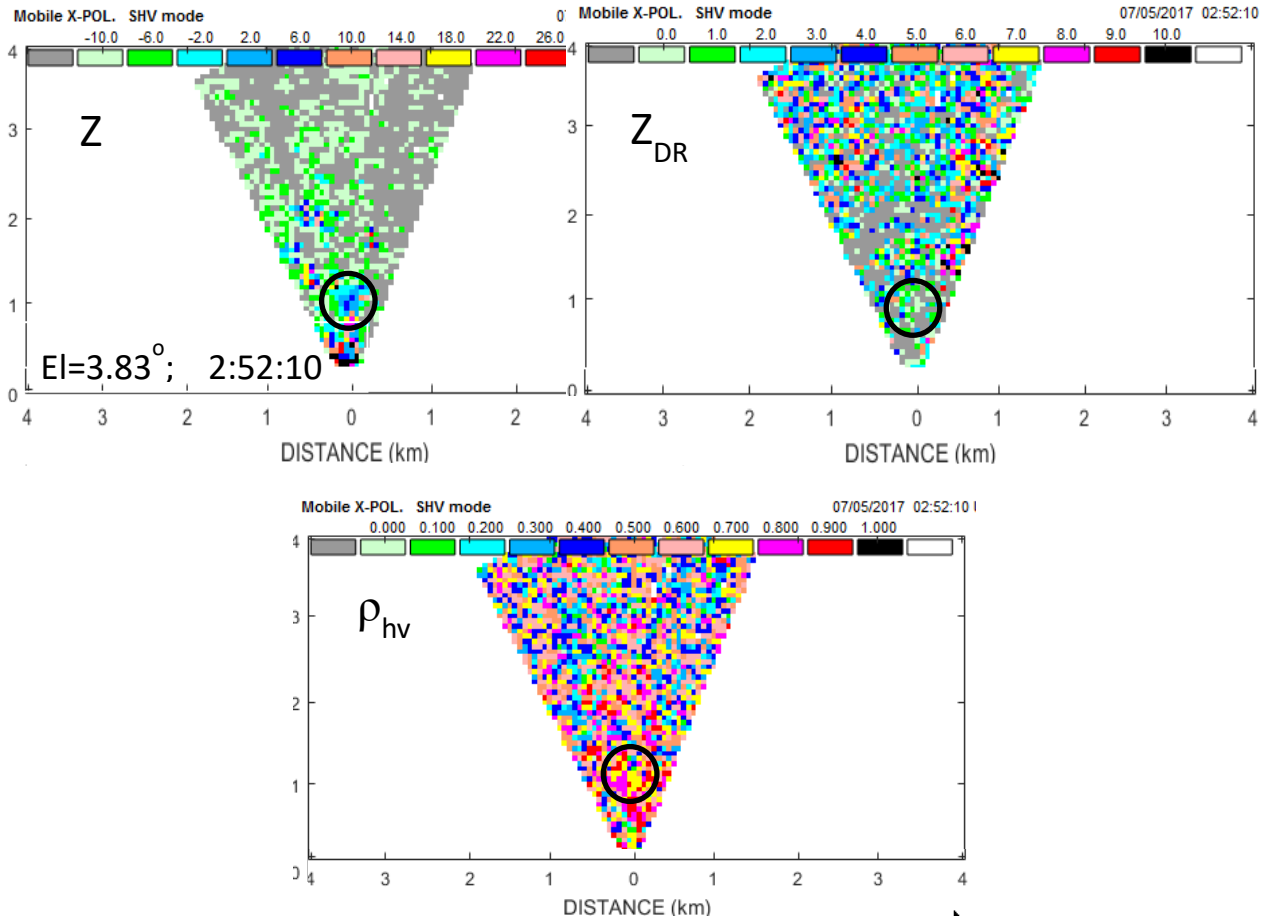

Fig. 17 The field of reflectivity factor (Z), differential reflectivity (Z_{DR}), and correlation coefficient ρ_{hv} at the elevation angle of 3.83º and about 2:52:10 UT, local time 9:52 pm July 4, 2017.

Lack of observation by KTLX we attribute to the 5 min sparse temporal sampling and beam height of 200 m above ground. Through contacts with the Radar Operation Center we have obtained data from their support WSR-88D radar called KCRI. Due to lack of time we did not analyze these data but intend to do so in the sequel report. The KCRI is only 200 m away from the KOUN hence its beam at the 0.5º elevation is 50 m above ground. It however has the same limitation in volume scan updates as the KTLX.

Last we present the reflectivity field (Fig. 18) obtained with the TDWR radar (location is in Fig. 15) for the Oklahoma City airport. Prior to the start of fireworks (at 2:39 UTC) there is no evidence of returns from the fireworks location. After the start of fireworks, the TDWR detects echoes at the correct location until the end of the event. In Fig. 18 are four images taken 6 min apart. The scan pattern consisted of volume updates at 6 min in which two scan at 0.5º elevation are repeated. These repeated scans are not shown here as they are redundant. The maximum reflectivity is 20.5 dBZ. There were no clear features in the velocity and spectrum width field that could be associated with the fireworks.

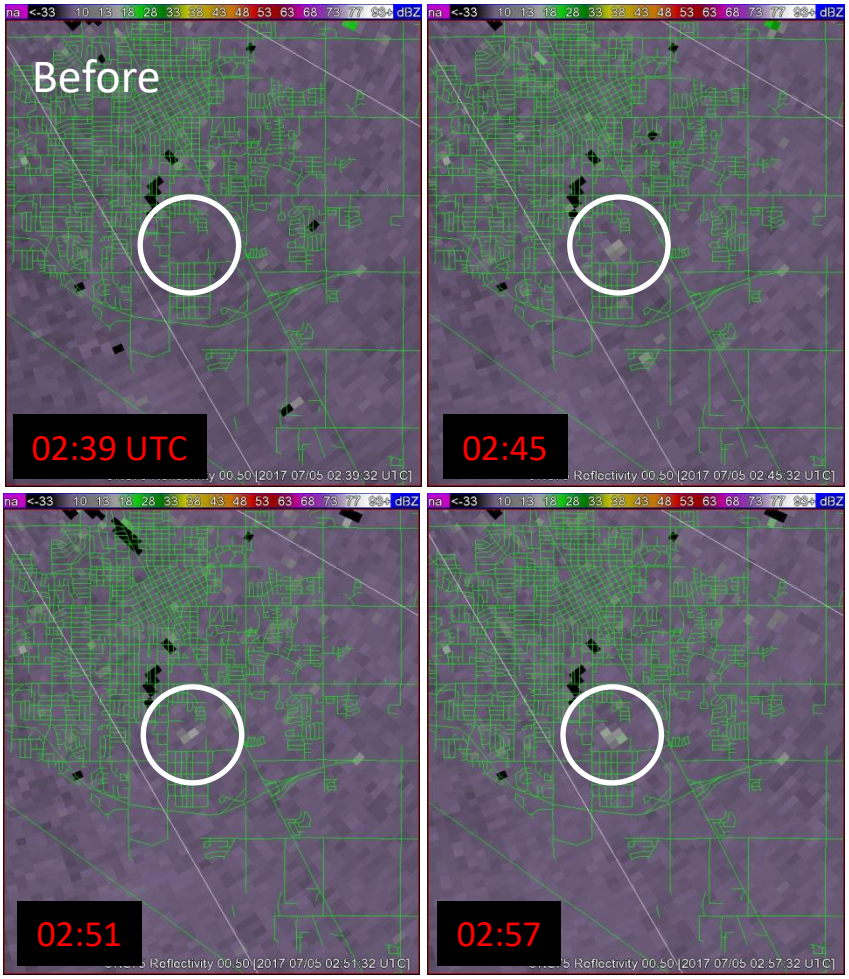

Fig. 18. Reflectivity field obtained from the TDWR radar on July Fourth 2017 (fifth according to UTC), at three different times. Elevation angle is 0.5º.

4. Recommendations

There is no doubt that detection on existing Level 2 data is feasible and could be achieved in practice fairly quickly if the data from the WSR-88D and the TDWR are used. Both these radars operate continuously, are well maintained as well as calibrated, and have provisions to provide Level 2 data. The WSR-88D has an advantage over the TDWR in that it is dual polarization radar. The number of WSR-88Ds is larger, about 160 compared to 47 of the TDWRs. The TDWRs advantages are its smaller beamwidth (0.5º vs 1º), more rapid update of lowest elevation scans (on average ~ 1min), and better detection capability (-26 dBZ at 10 km vs -21 dBZ) in the typical operation mode.

There are at least two possibilities on how and where to use the WSR-88D data. One is to install a processor at the location of the Radar Product Generator, ingest the Level 2 data and apply to it the Plume Detection Algorithm (PDA). The other possibility is to transmit the data from the RPG location to a location specified by DHS and process data there.

If the PDA is on a workstation collocated with the RPG it may be possible to obtain from the RPG additional data that could be incorporated into the PDA algorithm. For example, the

polarimetric data are preprocessed in the RPG. Preprocessing involves filtering of the Level 2 data, adding quality indexes, generating texture parameters of Z_{DR} and differential phase etc. These have been intensely vetted by the NWS and are one step behind the best that science can offer. Over time the NWS will change how it preprocesses the data on the basis of findings/suggestions by research organizations (NSSL/CIMMS, NCAR etc.). This will improve quality and usefulness of the data.

A potentially important aspect for the PDA could be to use the existing NWS algorithm that separates the data into "meteorological" and "non-meteorological". This algorithm, called MetSig (Krause 2016) exists on the RPG and would be improving and evolving over time. We envision a scenario whereby the PDA takes the non-meteorological data (the "Non MetSig)" and within these searches for the plume signatures. In addition, the PDA would use the preprocessed data. It could take into account spatial continuity, height above ground, and many other attributes that DHS would be developing. The advantage of this approach is in saving long term labor cost for maintaining a good part of the algorithm plus the latest and best of the preprocessing would be automatically added as the NWS makes the upgrades (planned at about 6 month intervals). For this option NWS would have to provide the preprocessed data which would be a onetime relatively small effort to make such stream available.

In summary the logistics on where to process the Level 2 data and generate value added information should be sorted out by the interested agencies. The point made here is that real time operation is feasible.

Currently an operational PDA algorithm does not exist. Nonetheless the MetSig algorithm classifies all non-meteorological returns into one category. Within this category the returns off plumes fall. It is therefore natural to search for plumes within this category. To do so one needs to quantify the range the polarimetric variables associated with plumes. This is achieved by computing histograms and scattergrams of data which are known to come from plumes. From this information one can build membership function, Bayes rules etc., or training sets for neural networks from which the plume class of echoes can be deduced.

Another meteorological feature useful for plume tracking is determination of the environmental wind field. The NWS has the Velocity Azimuth Display (VAD) algorithm which computes the vertical wind profile centered on the radar location. The algorithm preforms well if scatterers are fluctuations of refractive index or insects. During bird migration the VAD wind fields are contaminated by bird movement which is about 10 m s^{-1} higher than the environmental wind. It would be quite useful to separate the contribution by passive scatterers (such as insects) from active flyers (birds). One would need to censor data that go into this algorithm and modify the algorithms to look at close range (free of clutter) so that the winds near ground can be estimated.

There are other than VAD single Doppler wind retrieval methods (NSSL has a couple) that could be useful for retrieving winds. Also in areas where coverage by two radars overlaps it is possible to reconstruct the vector winds. This information could be useful for models that predict advection and dispersion of plumes.

References:

Billingsley J.B., 2002: Low Angle Radar Land Clutter. William Andrew publishing. Norwich, NY 13815. pp 703.

Francesc J., V. Chandrasekar, D. McLaughlin, E Insanic, and N. Bharadwaj, 2010: The CASA Integrated Project 1 Networked Radar System. *J. Atmos, Oceanic Technol.,* **27,** p. 62- 78.

Francesc J., V. Chandrasekar, D. Brunkow, P.C. Kennedy, D.J. McLaughlin, 2005: Validation of first generation CASA radars with CSU-CHILL. 32nd Conference on Radar Meteorology. AMS.

International Telecommunication Union Recommendation (ITU-R M.1313-1), 2000: Technical characteristics of maritime radio navigation radars.

Krause, J. M, 2016: A Simple Algorithm to Discriminate between Meteorological and Nonmeteorological Radar Echoes. *J. Atmos, Oceanic Technol.*, **33,** p. 1875- 1885.

Lakshmanan, V., C. Karstens, K. Elmore, A. Ryzhkov, and S. Berkseth, 2015: Which polarimetric variables are important for weather/no-weather discrimination? *J. Atmos. Oceanic Technol.*, **32,** 1209–1223.

Li L., G.M. Heymsfield, P.E. Racette, L. Tian, and E. Zenker, 2009: A 94-GHz Cloud Radar System on a NASA High-Altitude ER-2 Aircraft. *J. Atmos, Oceanic Technol.,* **21,** p. 1378-1388.

Melnikov, M.V., D.S. Zrnic, R.J. Doviak, P.B. Chilson, D.B. Mechem, and Y.L. Kogan, 2011: Prospects of the WSR-88D radar for cloud studies. *J. Appl. Meteor. Clim.,* **50,** 859-872.

Park, H., A. Ryzhkov, D. Zrnić, and K.-E. Kim, 2009: The hydrometeor classification algorithm for the polarimetric WSR-88D: Description and application to an MCS. *Wea. Forecasting*, **24,** 730–748,

Snyder, C. S, H. B. Vouestein, G. Zhang, and S. J. Frasier, 2010: Attenuation Correction and Hydrometeor Classification of High-Resolution, X-band, Dual-Polarized Mobile Radar Measurements in Severe Convective Storms. *J. Atmos, Oceanic Technol.,* **27,** p. 1979- 2001.

Zrnic, D., V. Melnikov, and R. J. Doviak, 2017: Capabilities of existing USA civilian radars to detect plumes, Report part I to the DOE, pp 23.

Zrnic, D.S., 1987: Three-Body Scattering Produces Precipitation Signatures of Special Diagnostic Value, *Radio Sci*., **22**, 76-86.